Understanding the complex structural features and phase changes in $Na_2Mg_2(SO_4)_3$: a combined single crystal and variable temperature powder diffraction and Raman spectroscopy study

I. A. Trussov[1], L. L. Male[1], M. L. Sanjuan[2], A. Orera[2] and P. R. Slater[1]

[1]*School of Chemistry, University of Birmingham, Birmingham, B15 2TT, UK*

[2]*Instituto de Ciencia de Materiales de Aragón (CSIC-Universidad de Zaragoza), 50009 Zaragoza, Spain*

Abstract

Sodium mixed metal sulphates have attracted considerable attention, both in terms of mineralogy and more recently due to interest in Na ion containing materials for battery applications. The phase, $Na_2Mg_2(SO_4)_3$, has been previously reported to undergo a phase change to langbeinite at high temperatures, which is interesting given that usually the langbeinite structure is only adopted when large alkali metal ions, e.g. K, Cs, are present. Nevertheless the room temperature structure of this phase has remained elusive, and so in this work, we report a detailed structural study of this system. We show that room temperature $Na_2Mg_2(SO_4)_3$ can only be prepared by quenching from high temperature, with slow cooling leading to phase separation to give the previously unreported systems, $Na_2Mg(SO_4)_2$ and $Na_2Mg_3(SO_4)_4$. We report the structures of quenched $Na_2Mg_2(SO_4)_3$ (monoclinic, $P2_1$), as well as $Na_2Mg(SO_4)_2$ (triclinic, $P\bar{1}$) and $Na_2Mg_3(SO_4)_4$ (orthorhombic, Pbca), detailing their complex structural features. Furthermore, we report a study of the thermal evolution of quenched $Na_2Mg_2(SO_4)_3$ with temperature through variable temperature XRD and Raman studies, which shows a complex series of phase transitions, highlighting why this phase has proven so elusive to characterise previously, and illustrating the need for detailed characterisation of such sulphate systems.

Keywords: sodium magnesium sulfate, langbeinite, nasicon, single crystal

1. Introduction

Interest in sodium metal sulphate materials has grown in the last decade as a consequence of interest resulting from the development of new cathode materials for Na ion batteries[1–9]. In this area, nasicon and alluaudite-type materials have been attracting considerable interest. The former systems have also been widely investigated for their ionic conductivity following the reports of excellent Na ion conduction in the nasicon-type phosphate-silicates, $Na_{1+x}Zr_2(PO_4)_{3-x}(SiO_4)_x$ [10–16]. In the case of sulphate systems, previous studies have shown that nasicon materials, $Na_xMg_xAl_{2-x}(SO_4)_3$, could be formed for $0 \leq x \leq 1.0$, with ionic conductivity increasing with Na content. The structure of these phases consists of a framework of corner linked Mg/AlO_6 and SO_4 tetrahedra, with the Na ions occupying cavity sites within this framework. Attempts to increase the Na content above x=1 led to the appearance of impurities. Nevertheless, the nominal x=2 phase, $Na_2Mg_2(SO_4)_3$, has been highlighted in the literature, having first been reported as an unknown mineral by Jacobsson et al. in 2008 [17]. This mineral was found in a sample from the Eldfell volcano eruption, albeit the composition and structure were not confirmed, and so the sample was simply labelled as "mineral EI". In later work, Balić-Žunić et al. reported the composition of this phase as $Na_2Mg_2(SO_4)_3$ from SEM studies, although they were unable to determine the room temperature structure[18]. Nevertheless, the authors did report interesting changes with temperature; in particular, above 550^{o}C the phase was observed to transform into the langbeinite structure with cubic space group $P2_13$. The results further showed that this high temperature langbeinite-type phase was non-quenchable, i.e. the cubic langbeinite

phase could not be obtained at room temperature by either slow or rapid cooling. The langbeinite structure shows some similarities with the structure of nasicon-type systems, in that it too consists of a framework of corner linked MgO_6 octahedra and SO_4 tetrahedra. However, for langbeinite, the cavity sites tend to be larger and so the structure is favoured by the presence of larger alkali ions such as potassium, caesium, and rubidium. Moreover, these two large cavity sites tend to be fully occupied, giving formulas such as $K_2Mg_2(SO_4)_3$ (the mineral langbeinite itself) [19,20]. The fact that an apparent langbeinite-type phase is observed for $Na_2Mg_2(SO_4)_3$ at elevated temperatures is therefore interesting, as sodium would normally be considered to be too small for the langbeinite structure, without the presence of additional larger ions to help to stabilise the structure [21,22].

The aim of this study was therefore to determine the room temperature structure of $Na_2Mg_2(SO_4)_3$ and account for the transformation to the langbeinite structure at elevated temperatures. Through these studies we have shown that the structural changes in this $Na_2Mg_2(SO_4)_3$ system are more complex than initially reported, and we clarify these complexities through single crystal and variable temperature powder X-ray diffraction and Raman spectroscopy studies, in order to provide a detailed understanding of this system. Given the complexities shown, the work suggests that similar more detailed variable temperature structural studies of other mixed metal sulphates are warranted.

2. Experimental details

$Na_2Mg_2(SO_4)_3$ powder samples were prepared via a dissolution-evaporation route by dissolving stoichiometric amounts of Na_2SO_4 and $MgSO_4{\cdot}7H_2O$ in water with

subsequent evaporation to produce the precursor mixture. This precursor mixture was reground and heated in air at 750°C for 12 hours. Two cooling regimes were examined, quenching (removal of the sample from the furnace at 750°C) and slow cooling in the furnace (1°C/min). Powder XRD data were collected on a Panalytical Empyrean diffractometer with copper X-ray source in reflection geometry equipped with Pixcel 2D detector. Variable temperature powder XRD data up to 750°C were collected on a Bruker D8 advanced diffractometer with copper X-ray source and LynxEye detector in an Anton Paar HTK1200N furnace. Rietveld refinement of powder XRD data was performed using GSAS-II software[23].

Single crystals were prepared by two methods. In the first instance it was found that small crystals could be found in the powder (quenched or slow cooled) samples prepared above. For the second method, crystals were grown via crystallisation from the melt at 900°C on gold foil with a subsequent cooling rate of 0.2°C/min in air. Single crystals were mounted on glass fibre and diffraction data were collected on an Agilent SuperNova diffractometer using an Atlas detector. The crystals were kept at 100K during data collection using an Oxford Cryosystems Cryostream. Due to the large complex triclinic unit cell, data for one single crystal ($Na_2Mg(SO_4)_2$) sample were collected (at 100K) by the UK National Crystallography Service [24] on a Rigaku FRE+ diffractometer equipped with rotating anode with VHF Varimax confocal mirrors, an AFC12 goniometer and HyPix 6000 detector. Using Olex2 [25], the structure was solved with the ShelXT[26] structure solution program using Intrinsic Phasing, and refined with the ShelXL [27] refinement package using a least squares approach.

Powder samples were also studied by means of Raman spectroscopy using the 488 nm excitation line of an Ar^+ ion laser in a DILOR XY spectrometer with a CCD detector with approximately 2 cm^{-1} of spectral resolution. The excitation and light

collection were made through a 50X microscope objective lens, meaning that a small sample region is analyzed at a time, and sampling was needed in order to confirm the homogeneity of the powder. High temperature Raman measurements were carried out in a LINKAM TS1500V stage up to 750°C, with the laser output power kept between 20 and 50 mW for measurements out/in the heating stage. Samples were also analyzed by thermal analysis (STA449 F1 Jupiter (Netzsch) TGA/DTA) to 750°C in N_2, heating at a rate of 5°C/min.

3. Results and discussion

3.*1. Initial results identifying the phase transitions*

In the preparation of $Na_2Mg_2(SO_4)_3$ powders it was found that depending on the cooling process two different results were obtained. In particular, it was shown that slow cooling in air led to a mixture of two phases (indicating phase separation), while quenching led to single phase $Na_2Mg_2(SO_4)_3$ (Figure 1). The quenched $Na_2Mg_2(SO_4)_3$ phase was shown to be a new phase, monoclinic ($P2_1$) $Na_2Mg_2(SO_4)_3$, from the structural analysis using single crystal data (discussed later).

In contrast to the single phase monoclinic $Na_2Mg_2(SO_4)_3$ obtained on quenching,

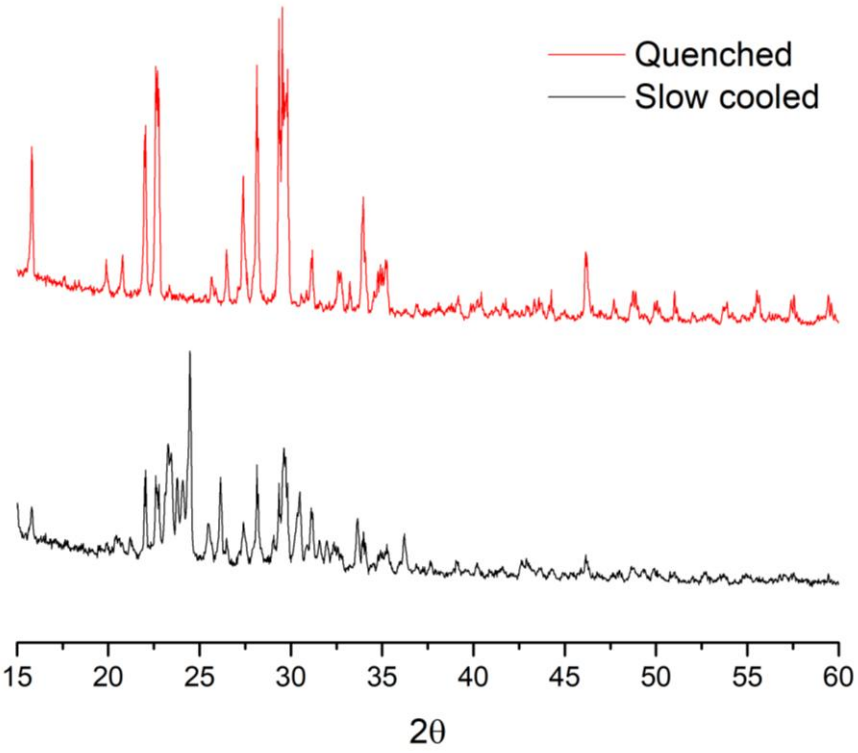

Figure 1. XRD patterns of $Na_2Mg_2(SO_4)_3$ at room temperature after quenching ($Na_2Mg_2(SO_4)_3$ phase maintained) and slow cooling (phase separation of $Na_2Mg_2(SO_4)_3$ into $Na_2Mg_3(SO_4)_4$ and $Na_2Mg(SO_4)_2$

the slow cooled sample shows a mixture of two phases. Via extraction of single crystals from a slow cooled melt we were able to identify these two phases and determine their crystal structures through single crystal XRD analysis. These two phases were identified as orthorhombic (Pbca) $Na_2Mg_3(SO_4)_4$ and triclinic ($P\bar{1}$) $Na_2Mg(SO_4)_2$, both of which have not been previously reported. The results therefore indicate that $Na_2Mg_2(SO_4)_3$ decomposes during the slow cooling process, and so an overall phase scheme for the "$Na_2Mg_2(SO_4)_3$" system can be described as below:

$$\begin{matrix}\frac{1}{2}Na_2Mg_3(SO_4)_4\ (Pbca)\\ \frac{1}{2}Na_2Mg(SO_4)_2\ (P\bar{1})\end{matrix} \xleftarrow{\text{Slow cooling}} Na_2Mg_2(SO_4)_3\ (750^oC) \xrightarrow{\text{Quenching}} Na_2Mg_2(SO_4)_3\ (P2_1)$$

In order to gather further information on the phase changes in this "$Na_2Mg_2(SO_4)_3$" system, variable temperature powder XRD (Figure 2) studies were performed. These studies showed similar results to those previously reported by Balić-Žunić et al.[18], with the transformation of both the low temperature systems (quenched and slow cooled) into the cubic langbeinite ($P2_13$) $Na_2Mg_2(SO_4)_3$ structure at a temperature near 600°C during the heating stage (Figure 2).

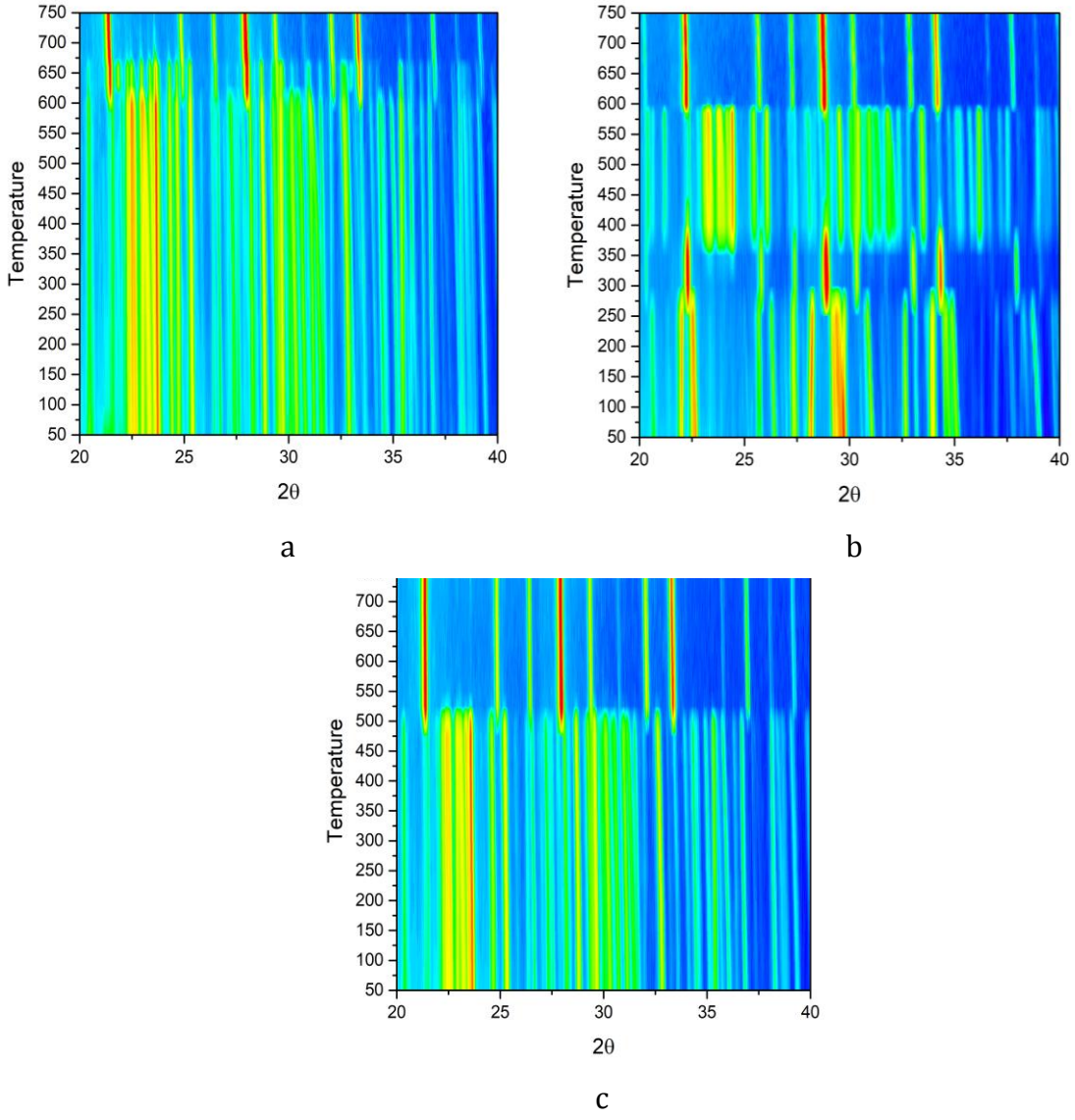

Figure 2. Contour plots for variable temperature XRD of $Na_2Mg_2(SO_4)_3$ compositions: a) heating the slow cooled sample (mixture of $Na_2Mg_3(SO_4)_4$ and $Na_2Mg(SO_4)_2$) shows one transition caused by reaction of components to give langbeinite-type $Na_2Mg_2(SO_4)_3$, b) heating the quenched ($Na_2Mg_2(SO_4)_3$) phase shows a range of different transitions caused by phase transformation and decomposition/recombination of components, c) slow cooling samples show a single decomposition point at ≈525°C into a mixture of $Na_2Mg_3(SO_4)_4$ and $Na_2Mg(SO_4)_2$.

In the case of the slow cooled decomposed mixture of $Na_2Mg_3(SO_4)_4$ and $Na_2Mg(SO_4)_2$, we observe a simple reaction between these component phases resulting in the formation of the langbeinite $Na_2Mg_2(SO_4)_3$ phase, starting at 610°C . This is a slow process, as highlighted by the fact that we can still observe peaks due to the starting

phases in the pattern up to 675°C (Figure 2a). The cooling stage of the variable temperature data highlights that, on slow cooling, decomposition of the langbeinite-type, $Na_2Mg_2(SO_4)_3$ phase to $Na_2Mg_3(SO_4)_4$ and $Na_2Mg(SO_4)_2$ occurs at ≈525°C (Figure 2c).

The variable temperature powder XRD studies on the quenched monoclinic $Na_2Mg_2(SO_4)_3$ phase, showed a different thermal behaviour on heating. This phase first transforms into a cubic langbeinite phase at ≈250°C, and then decomposes at ≈350°C into the $Na_2Mg_3(SO_4)_4$ and $Na_2Mg(SO_4)_2$ mixture (Figure 2b). On heating to higher temperature, this $Na_2Mg_3(SO_4)_4$ and $Na_2Mg(SO_4)_2$ mixture recombines (at ≈575°C) to give cubic langbeinite-type $Na_2Mg_2(SO_4)_3$ again. The whole variable temperature phase transformation process for quenched $Na_2Mg_2(SO_4)_3$ can thus be expressed with the following scheme:

$$\text{Monoclinic } P2_1 \xrightarrow{250^{\circ}C} \text{Langbeinite } P2_13 \xrightarrow{350^{\circ}C} \text{Mixture } Pbca + P\bar{1} \xrightarrow{575^{\circ}C} \text{Langbeinite } P2_13$$

In this case reaction between $Na_2Mg_3(SO_4)_4$ and $Na_2Mg(SO_4)_2$ occurs completely after reaching 575°C, a slightly lower temperature than previously for the slow cooled system. The reason for this lower temperature is most likely related to the highly homogeneous distribution of the compounds after phase decomposition of the lower temperature langbeinite phase.

In addition to analysing $Na_2Mg_2(SO_4)_3$ we also managed to synthesise the pure triclinic $Na_2Mg(SO_4)_2$ phase by slow cooling (1°C/min) 1:1 mixtures of Na_2SO_4 and $MgSO_4$ from 650°C. Interestingly, relatively rapid cooling pf this phase gives a mixture of vantgoffite $Na_6Mg(SO_4)_4$ and $MgSO_4$. The thermal evolution of this $Na_2Mg(SO_4)_2$ phase is also interesting (Figure 3). In particular, high temperature powder XRD suggests that this phase decomposes at ~625°C into a langbeinite phase ($a_{923K} = 9.855(1)$Å), and an extra phase which is related to the high temperature form of vantgoffite $Na_6Mg(SO_4)_4$ (triclinically distorted hexagonal lattice a=5.292(7)Å, b=7.775(3)Å, c=5.413(7)Å,

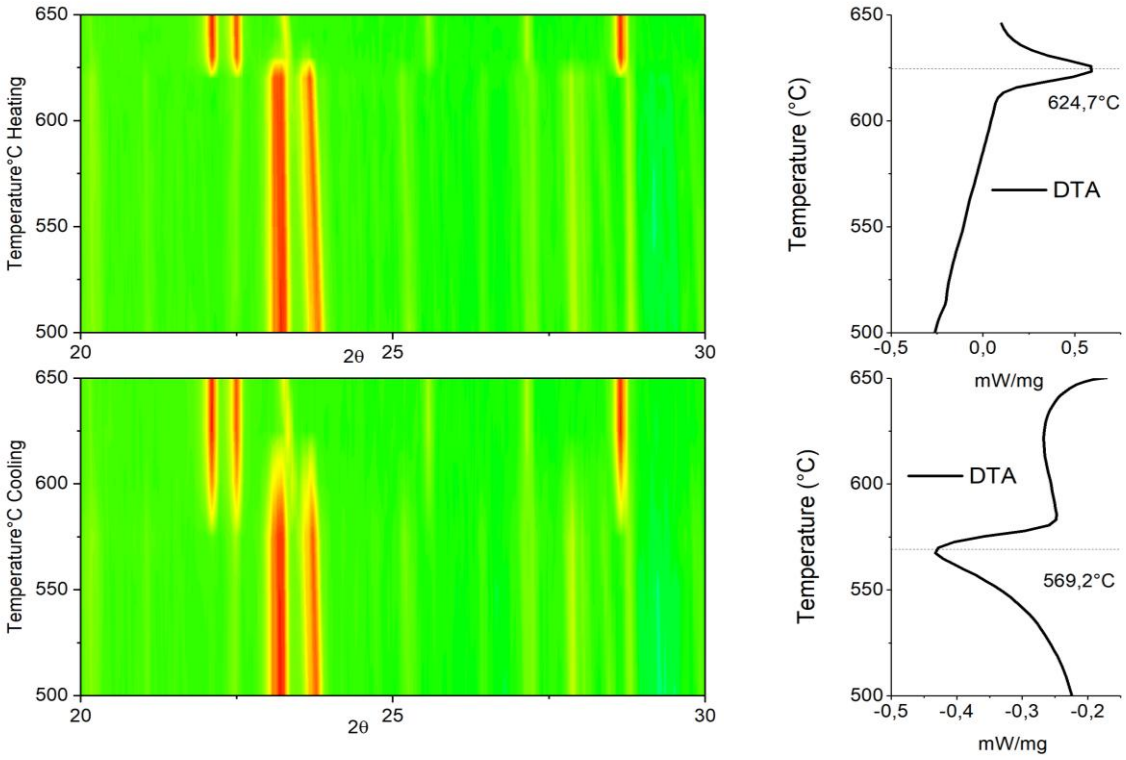

Figure 3. Contour plots of variable temperature XRD and DTA curves of $Na_2Mg(SO_4)_2$ showing a decomposition into langbeinite-type $Na_2Mg_2(SO_4)_3$ and high temperature vantgoffite $Na_6Mg(SO_4)_4$ at elevated temperature on heating, with a recombination on cooling to give $Na_2Mg(SO_4)_2$. For the latter, slow kinetics for this process means that there is a small range of temperatures where all three phases are present. Note the difference in temperature between the phase transition in XRD and DTA relates to these slow kinetics and the fact that the latter cooling stage corresponds to a faster rate

α=89.62(3)^{o}, β=91.25(5)^{o}, γ=119.34(3)^{o}). On cooling these two phases recombine to form the original $Na_2Mg(SO_4)_2$ although slow kinetics leads to incomplete reaction/recombination for samples which are cooled rapidly, and so consequently slow cooling is required to produce pure $Na_2Mg(SO_4)_2$. These slow kinetics are highlighted in the variable temperature XRD data on cooling, which show that there is a small range of temperatures where all three phases are present.

3.2. Single crystal study

Due to issues with the decomposition of $Na_2Mg_2(SO_4)_3$ into $Na_2Mg_3(SO_4)_4$ and $Na_2Mg(SO_4)_2$ on slow cooling, it was not possible to grow single crystals of this compound from a slow cooled melt. Nevertheless, we were able to pick a small single crystal of monoclinic $Na_2Mg_2(SO_4)_3$ from the freshly quenched powder.

Single crystals of orthorhombic $Na_2Mg_3(SO_4)_4$ and triclinic $Na_2Mg(SO_4)_2$ were grown from the melt at 900°C on gold foil. In the case of the former, a small single crystal of the orthorhombic $Na_2Mg_3(SO_4)_4$ phase was picked from a decomposed slow cooled melt of initial composition $Na_2Mg_2(SO_4)_3$. The triclinic $Na_2Mg(SO_4)_2$ crystal was grown from a slow cooled melt of the premade pure powder $Na_2Mg(SO_4)_2$ phase.

Due to the rather large and relatively simple orthorhombic cell, a copper X-ray tube was selected for the data collection on the $Na_2Mg_3(SO_4)_4$ crystal. Data collection for the monoclinic $Na_2Mg_2(SO_4)_3$ single crystal was more complicated because of the chirality of the cell and non-merohedral twinning of the single crystal. To handle this the whole diffraction sphere of the data was collected with a molybdenum X-ray source. No specific restraints were used for structural refinement.

Data collection for the triclinic $Na_2Mg(SO_4)_2$ phase proved to be a challenging task, given the complexity of the structure and the small size of the single crystal. In this case, collection of the whole diffraction sphere was performed with a molybdenum X-ray source. However, it was found that the crystal structure didn't produce many strong reflections, which meant that we were unable to collect sufficient amount of data in adequate time on our in-house diffractometer. In order to solve this issue, crystals of the $Na_2Mg(SO_4)_2$ phase were sent to the UK National Crystallography Service (Southampton, UK) for data collection. For this system, it was found that the standard single crystal

growth process is not efficient and during the high temperature synthesis process (complexities of phase formation noted in the variable temperature powder diffraction study) the crystals are formed with some defects. Therefore the data were collected on a non-merohedrally twinned crystal with one significant domain and several much smaller domains. It was found best to treat the main domain as if it were a dataset from a single crystal. This treatment of the data allowed us to successfully solve the structure. The main information for the single crystal experiments and results are shown in table 1 (the full refined structural parameters are given in supplementary information).

Table 1. Single crystal study information

Empirical formula	$Mg_2Na_2O_{12}S_3$	$Mg_3Na_2O_{16}S_4$	$MgNa_2O_8S_2$
Formula weight	382.78	503.15	262.41
Temperature/K	100.00(10)	100.00(10)	100(2)
Crystal system	monoclinic	orthorhombic	triclinic
Space group	$P2_1$	Pbca	P-1
a/Å	13.6986(3)	9.51764(19)	11.14950(10)
b/Å	9.5323(2)	8.70474(15)	13.42540(10)
c/Å	21.3167(4)	29.1089(6)	16.9497(2)
α/°	90	90	99.7390(10)
β/°	105.114(2)	90	106.9960(10)
γ/°	90	90	105.2980(10)
Volume/Å^3	2687.23(10)	2411.63(8)	2255.40(4)
Z	12	8	14
ρ_{calc}g/cm^3	2.838	2.772	2.705
μ/mm^{-1}	1.138	10.567	1.068
F(000)	2280	2000	1820
Crystal size/mm^3	0.092 × 0.082 × 0.057	0.238 × 0.171 × 0.113	0.11 × 0.09 × 0.05
Radiation	MoKα (λ = 0.71073)	CuKα (λ = 1.54184)	MoKα (λ = 0.71075)
2Θ range for data collection/°	4.336 to 64.062	11.108 to 139.948	3.264 to 61.012
Index ranges	-20 ≤ h ≤ 20, -14 ≤ k ≤ 14, -31 ≤ l ≤ 31	-11 ≤ h ≤ 7, -10 ≤ k ≤ 10, -35 ≤ l ≤ 20	-15 ≤ h ≤ 15, -19 ≤ k ≤ 19, -24 ≤ l ≤ 24
Reflections collected	36911	6016	155205
Independent reflections	36911 [R_{sigma} = 0.0613]	2274 [R_{int} = 0.0194, R_{sigma} = 0.0200]	13757 [R_{int} = 0.0456, R_{sigma} = 0.0177]
Data/restraints/ parameters	36911/1/1028	2274/0/226	13757/25/870

Goodness-of-fit on F^2	0.977	1.055	1.032
Final R indexes [I>=2σ (I)]	R_1 = 0.0310, wR_2 = 0.0643	R_1 = 0.0246, wR_2 = 0.0666	R_1 = 0.0367, wR_2 = 0.0835
Final R indexes [all data]	R_1 = 0.0398, wR_2 = 0.0655	R_1 = 0.0263, wR_2 = 0.0678	R_1 = 0.0399, wR_2 = 0.0851
Largest diff. peak/hole e/Å^3	0.54/-0.53	0.40/-0.55	3.69/-2.38
Flack parameter	-0.02(3)	n/a	n/a
CCDC deposition number	CCDC 1881701	CCDC 1881700	CCDC 1881702

3.3. Monoclinic $Na_2Mg_2(SO_4)_3$

The quenched sample of $Na_2Mg_2(SO_4)_3$ was shown to be monoclinic with space group $P2_1$. The cell is relatively complex and the whole structural pattern becomes clear only on examination of an enlarged supercell. The chiral structure consists of SO_4 tetrahedra corner sharing with MgO_6 or MgO_5 units. The latter MgO_5 units are mostly distorted square pyramids, although one in every three units adopts a more trigonal bipyramid arrangement due to local distortions. The distorted square pyramids have a

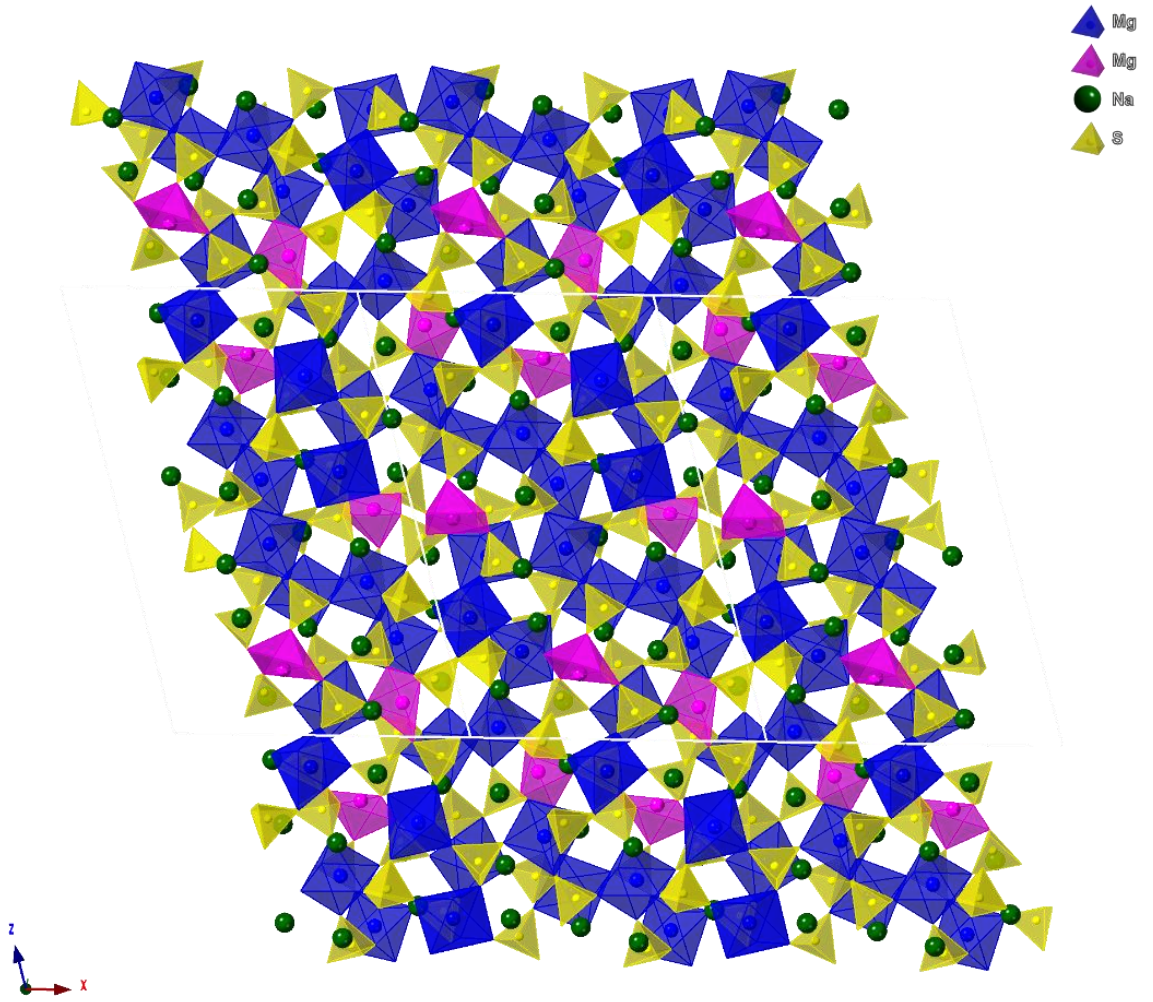

Figure 4. Single crystal structure of $Na_2Mg_2(SO_4)_3$ at 100K

dipole moment with positive base and negative top corner. These MgO_5 units are gathered in two types of clusters in the crystal lattice (Figure 4).

The first type is a cluster of two square pyramids with non-parallel base-facing. These double pyramid clusters, via symmetry, form a surface in the (0 0 2) plane with polarisation vector along the *b* axis. The second cluster consists of an aggregation of four MgO_5 units forming helixes with positive polarisation in the centre directed along the axis of the helix (Figure 5). The resultant stack of helixes forms a layer in the (0 0 1) plane. In total the structure consists of alternating parallel layers of helixes and double pyramid clusters. The overall polarisation vectors of both cluster systems are collinear. A close inspection of the MgO_5 square pyramids shows that they can also be described as distorted MgO_6 octahedra with one of oxygen atoms at a significantly longer distance. This can be illustrated by Figure 6, which shows the distribution of interatomic distances (with Gaussian fitting) at room temperature surrounding the magnesium. The main peak in the interatomic distances around Mg can be described with a peak at 2.02Å corresponding to the expected Mg-O distance. However an extra peak is observed

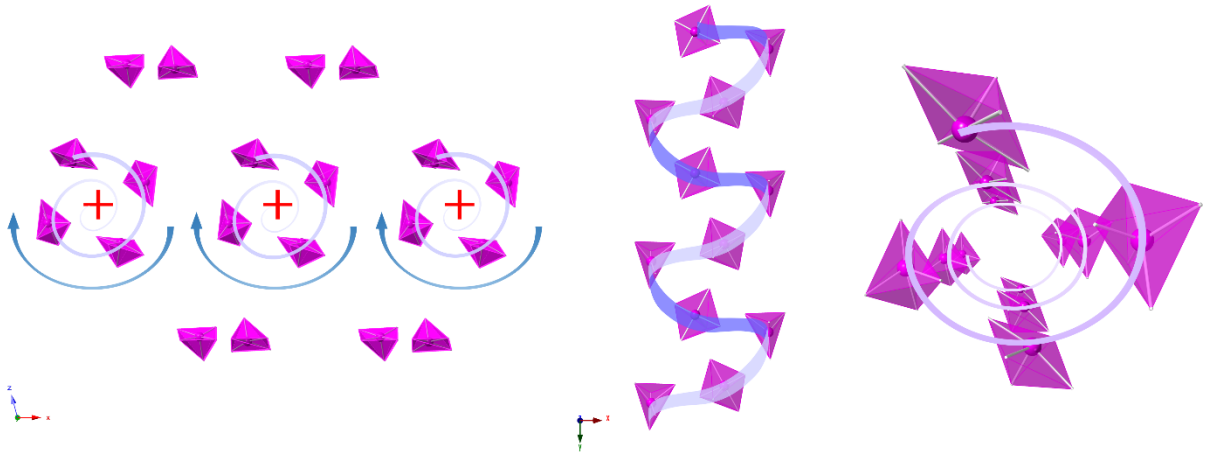

Figure 5. (left image) The orientations of MgO_5 pyramids forming helixes in monoclinic $Na_2Mg_2(SO_4)_3$ (100K). Arrows show the downwards rotation of the helixes forming the layer. Double pyramid clusters layers are above and below the helix layer;
(middle image) Illustration of a single helix in profile;
(right image) An enlarged top view of the helix showing the spiralling of the

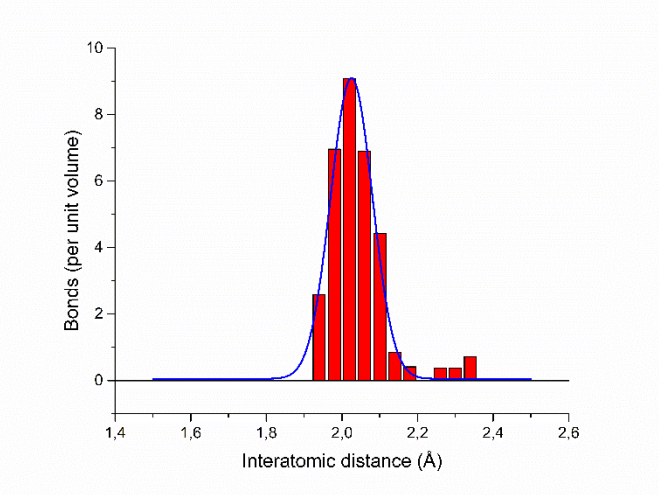

Figure 6. Distribution of interatomic distances (with Gaussian fitting) surrounding Mg in quenched $Na_2Mg_2(SO_4)_3$.

at around 2.3 Å corresponding to the longer bond to the oxygen atom making up the sixth bond to the MgO_5 units.

The low temperature phase transition to cubic langbeinite can be explained by the fact that, despite the apparent complex structure of $Na_2Mg_2(SO_4)_3$, in reality this phase is similar to langbeinite in that it requires only a small amount of rotation of the SO_4 units in langbeinite to conduct the change of the cell symmetry (cubic-monoclinic). The variable temperature data shows, however, that the structure is unstable at intermediate (≈350-≈600°C) temperatures, and so it decomposes into the two compounds $Na_2Mg_3(SO_4)_4$ and $Na_2Mg(SO_4)_2$. This phase decomposition is a complex process and so has relatively slow kinetics, and so the $Na_2Mg_2(SO_4)_3$ phase can be preserved at low temperatures by quenching. It is possible that the decomposition into $Na_2Mg_3(SO_4)_4$ and $Na_2Mg(SO_4)_2$ might also be avoided on heating by using rapid heating rates.

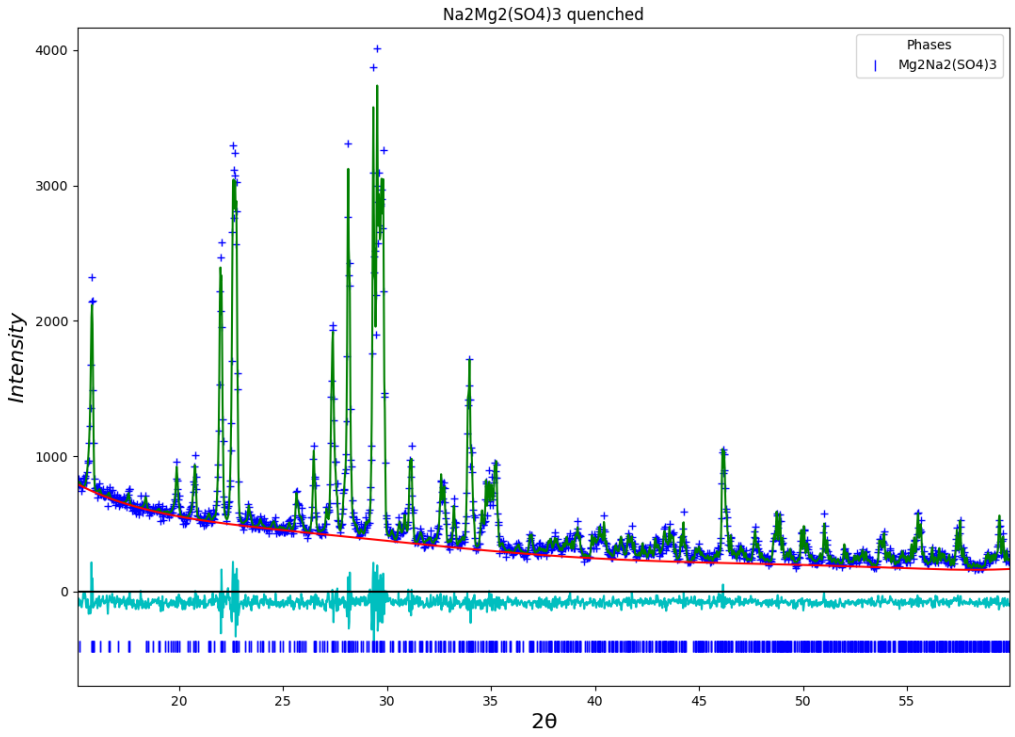

Figure 7. Observed, calculated and difference plots for structural refinement of quenched $Na_2Mg_2(SO_4)_3$ using X-ray powder diffraction data

In order to confirm that the quenched $Na_2Mg_2(SO_4)_3$ powder was indeed monoclinic $Na_2Mg_2(SO_4)_3$, a basic Rietveld refinement was performed using the powder XRD data (using the single crystal structural parameters for monoclinic $Na_2Mg_2(SO_4)_3$). This refinement led to a good fit to the data, thus confirming that the quenched powder was indeed monoclinic $Na_2Mg_2(SO_4)_3$ (Figure 7).

3.4. $Na_2Mg_3(SO_4)_4$

The single crystal data showed that $Na_2Mg_3(SO_4)_4$ has an orthorhombic cell with space group Pbca. The crystal structure consists of SO_4 tetrahedra corner sharing with MgO_6 or MgO_5 units. All the SO_4 tetrahedra are relatively undistorted and the average S-O bond length is 1.472 Å. The magnesium atoms in this system occupy three different sites. On the first site, Mg1, magnesium is six-coordinate and forms MgO_6

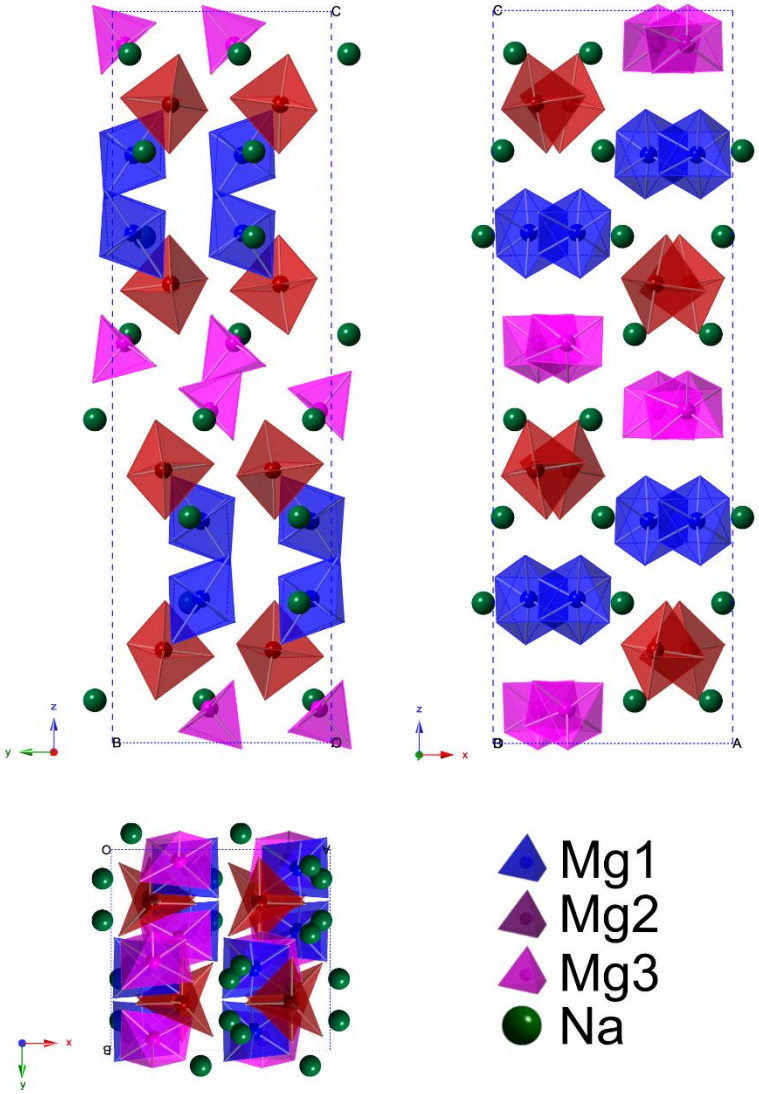

Figure 8. Structure of $Na_2Mg_3(SO_4)_4$ with different plane projections. SO_4 units are omitted for clarity. Top left – view along the *a* axis, top right – view along *b* axis, bottom – view along *c* axis.

octahedra, where all the Mg-O bonds have similar lengths in the equatorial plane around 2.038 Å, while the axial oxygen atoms are at a slightly longer average distance of 2.128 Å. For the Mg2 site, magnesium is five-coordinate trigonal bipyramidal. The central oxygen triangle is close to being isosceles with dimensions 2.38-2.95-3.07Å. The distances from Mg2 to O are also relatively similar - 2.02 Å. The third magnesium site, Mg3, is also five-coordinate, but in this case the MgO_5 unit forms a square pyramid. All the Mg-O distances in the pyramid are roughly the same. Moreover, the four oxygen torsion angles within the pyramid base do not exceed 2˚, i.e. the base surface is fairly flat. The absence of the sixth oxygen leads to a Mg-O dipole, which causes polarisation of the adjacent MgO_6 octahedra as illustrated by the longer Mg-O_{axial} bond, and results in a long range (3.036Å) interaction of this axial O with the MgO_5 pyramid (Figure 9).

The overall crystal structure can be considered as layered. It consists of four symmetrical triple-layers of Mg1-Mg2-Mg3 units. Within each triple-layer MgO_5 square pyramids are collinear and point in the same positive direction at 42.4° towards the centre of the layer. The dipole vectors of the MgO_5 bipyramids alternate with 69.1° difference and therefore the resulting dipole vector is non-zero (Figure 10). The next triple layer is the exact mirror reflection of the first layer along the plane perpendicular to *c* axis, beginning with the MgO_6 octahedra followed by the MgO_5 bipyramids and finishing with the MgO_5 square pyramids. The total

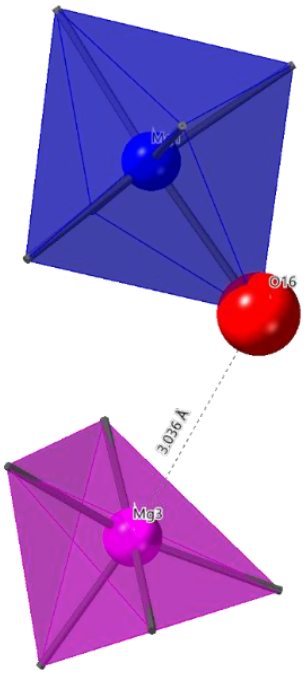

Figure 9. Arrangement of the MgO_6 octahedra and MgO_5 pyramid

dipole vector of the first two triple-layers associated with the MgO_5 units is non-zero and lies parallel to the *b* axis. The next two layers are a centrosymmetric reflection of first two. Thus they have the same total dipole vector but with an opposite direction, resulting in the dipole sum over all four layers being equal to zero. This complex structural arrangement thus explains the rather large unit cell parameters for this compound. The differently oriented dipoles in this structure suggest an interesting 3D-landscape of local polarisations, which may be of interest for future dielectric studies.

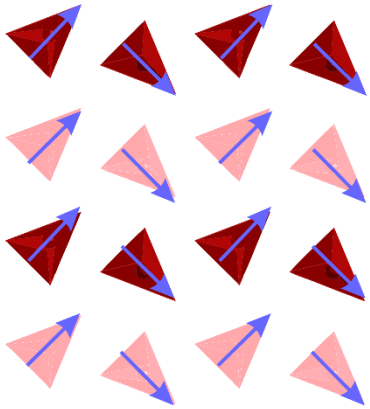

Figure 10. Arrangement of bipyramids in half of the lattice. Dark and pale colours represent different levels of the lattice. Arrows show vector of positive polarisation

The calculated bond valence sum (BVS) for the Mg2 and Mg3 sites are close to ideal at +2.005 and +1.995 respectively, which explains the stability of these five coordinate units. The BVS for the octahedral Mg1 site is, however, lower than expected: +1.869, which may be the result of the polarisation caused by the adjacent MgO_5 pyramid as highlighted above (Figure 9).

Examination of $Na_2Mg_3(SO_4)_4$ through VT-XRD experiments shows that unlike $Na_2Mg_2(SO_4)_3$ or $Na_2Mg(SO_4)_2$, there are no phase transitions with temperature up to 750°C.

3.5. $Na_2Mg(SO_4)_2$

Structure refinement using the single crystal data indicated that the $Na_2Mg(SO_4)_2$ phase is triclinic with space group P-1. The unit cell mostly consists of SO_4 tetrahedra corner linked with MgO_6 octahedra, with the sodium ions distributed in the resultant network. The view along the vector perpendicular to the plane (-4 0 -5) implies a hexagonal pattern structure similar to that of the Nasicon structure (Figure

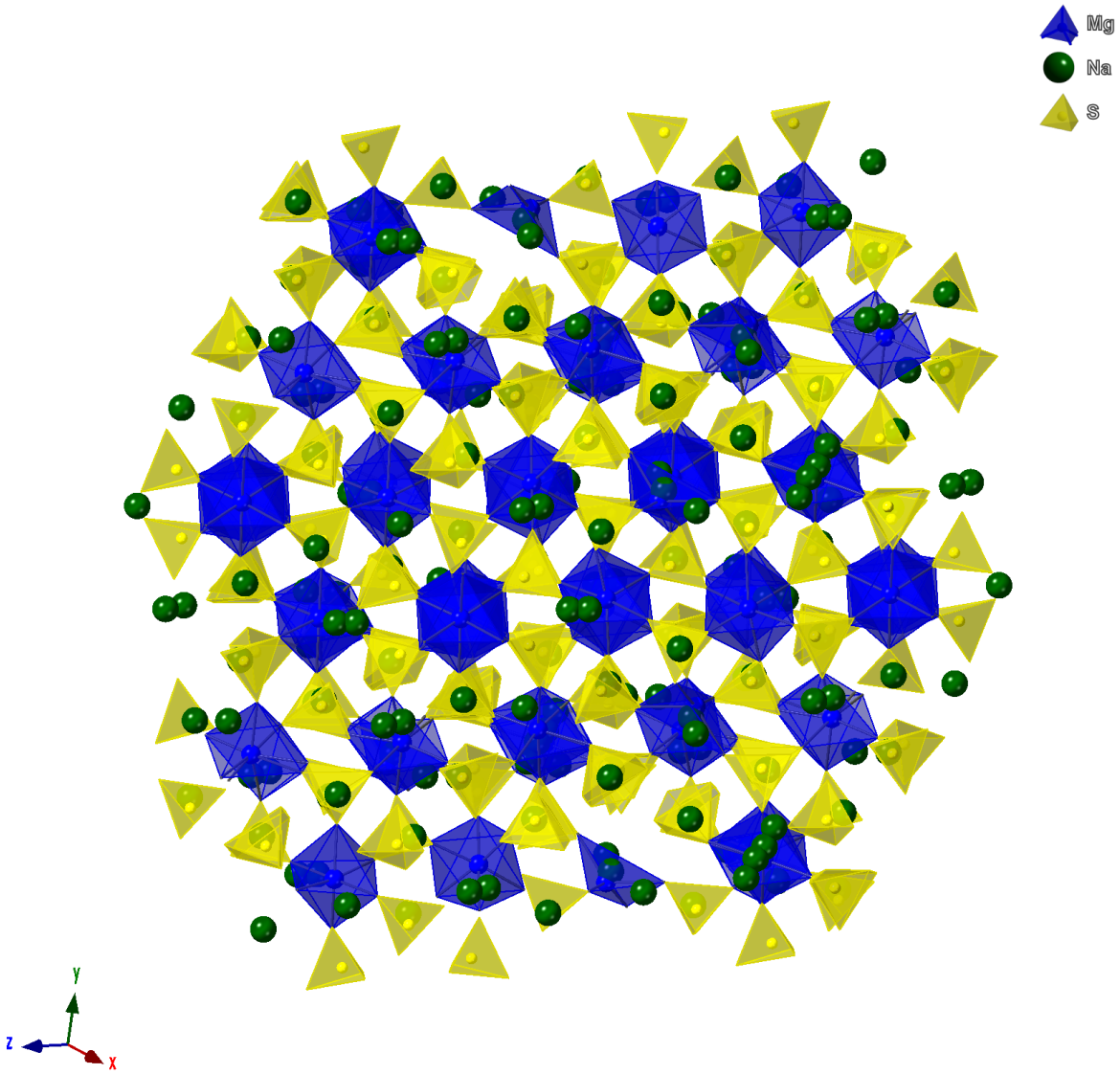

Figure 11. Structure of $Na_2Mg(SO_4)_2$ viewed perpendicular to plane (-4 0 -5)

11). However the crystal slice along the (1 -3 0) plane perpendicular to (-4 0 -5) shows a different pattern. While this has some elements similar to the Nasicon structure, such as two octahedral MgO_6 units linked via three tetrahedral SO_4 units (Nasicon lantern unit [28])(Figure 12, red selection), the presence of some Na occupying Mg sites causes deformation and disorder in the cell. In these regions, the structure is more similar to the Na rich Vantgoffite ($Na_6Mg(SO_4)_4$) phase, where MgO_6 units are surrounded by Na ions with interstitial SO_4 tetrahedra (Figure 12, black selection). These areas can be classed as large cavities containing sodium ions, and the sulphate groups are rotationally distorted when surrounded by a large amount of Na ions in these regions. The presence of large disorder of the Na in the structure may suggest that this material might show significant ionic mobility. Furthermore, possible spontaneous polarisation within this structure can be generated via disordering and lowering the symmetry to P1, i.e. if Na ions would tend to occupy the same pole of the large cavities.

Indeed, while we have produced a good solution to the structure with space group $P\bar{1}$, the symmetry may possibly be lower (P1). Twinning artefacts from the data set may have affected the structure solution, causing the extra visual disorder. Indeed, the presence of large amounts of disorder, as well as mixed Na/Mg occupied sites across the centre of symmetry (pink labelled Mg8), may suggest that the space group is P1 rather than of $P\bar{1}$. The main difficulty in providing a conclusive description either way is the mixed Na/Mg occupied sites. The scattering factors of these elements are essentially identical and so normally the only way to distinguish them is to compare the bond lengths. However, the large degree of complexity within this structure makes such an

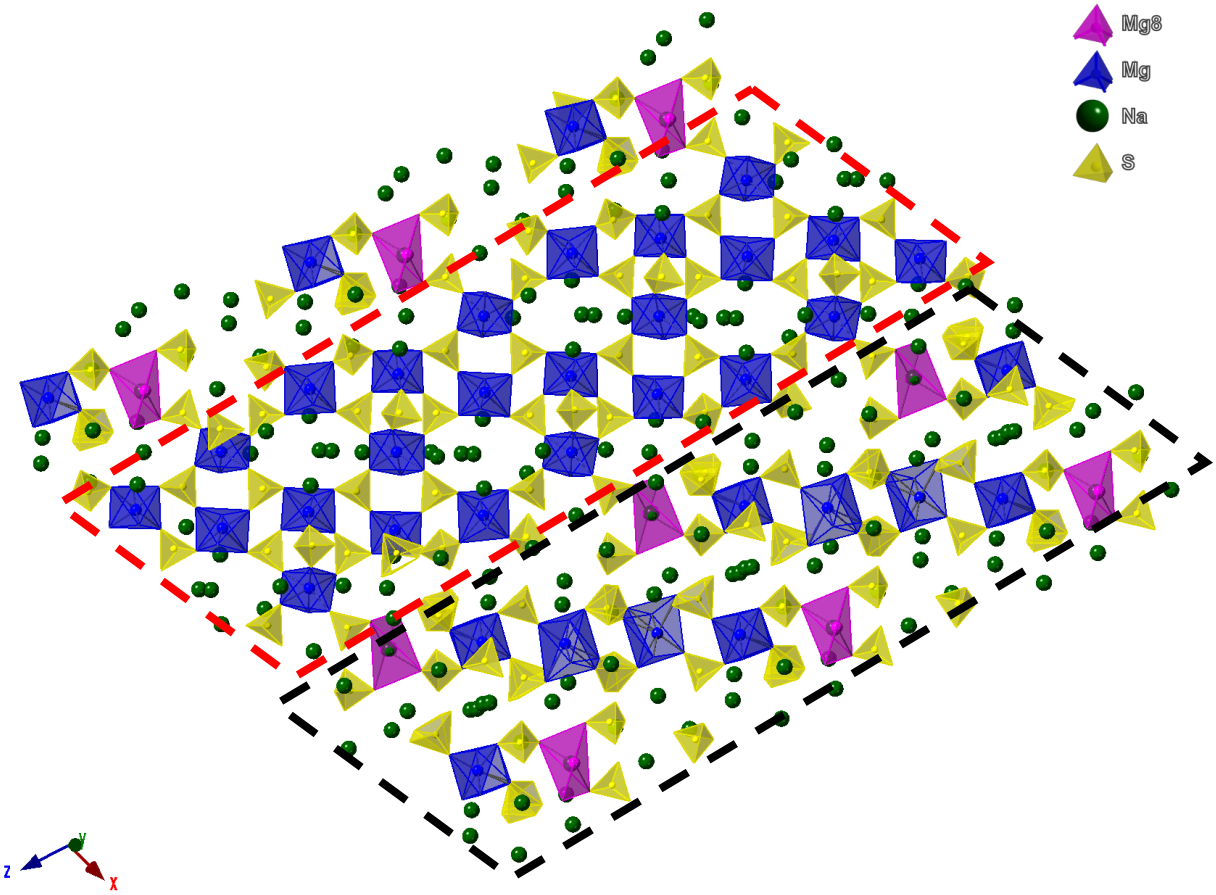

Figure 12. $Na_2Mg(SO_4)_2$ structure slice along (1 -3 0). Mg8 site labelled pink. The region that is similar to Nasicon is highlighted by the red dash line. The vantgoffite-like region is highlighted by the black dash line.

analysis impractical, and so we have kept the higher symmetry $P\bar{1}$ description. In order, to fully distinguish between these two possibilities, a neutron single crystal diffraction study would be required. However this method requires a much larger single crystal which has not been achievable via the current synthesis route.

3.6. Raman Spectroscopy study

Further information about the thermal structure evolution of $Na_2Mg_2(SO_4)_3$ was obtained from Raman scattering measurements. Some hydration was observed in the stored samples, as denoted by the presence of a broad band in the 3500 cm^{-1} region as well as some narrow bands around 1000 cm^{-1} with variable intensity which did not belong to the proper $Na_2Mg_2(SO_4)_3$ phase. In order to avoid any humidity effect, the samples were thermally treated at 700ºC in the measuring stage under an air flow just before the Raman measurements. Figure 13 shows the Raman spectrum of dried $Na_2Mg_2(SO_4)_3$, and although an exhaustive mode assignment is out of the scope of the present work, we identify the bands in the 460, 630, 1040 and above 1100 cm^{-1} regions as corresponding to the ν_2 (symmetric bending), ν_4 (antisymmetric bending), ν_1 (symmetric stretching) and ν_3 (antisymmetric stretching) internal modes of the

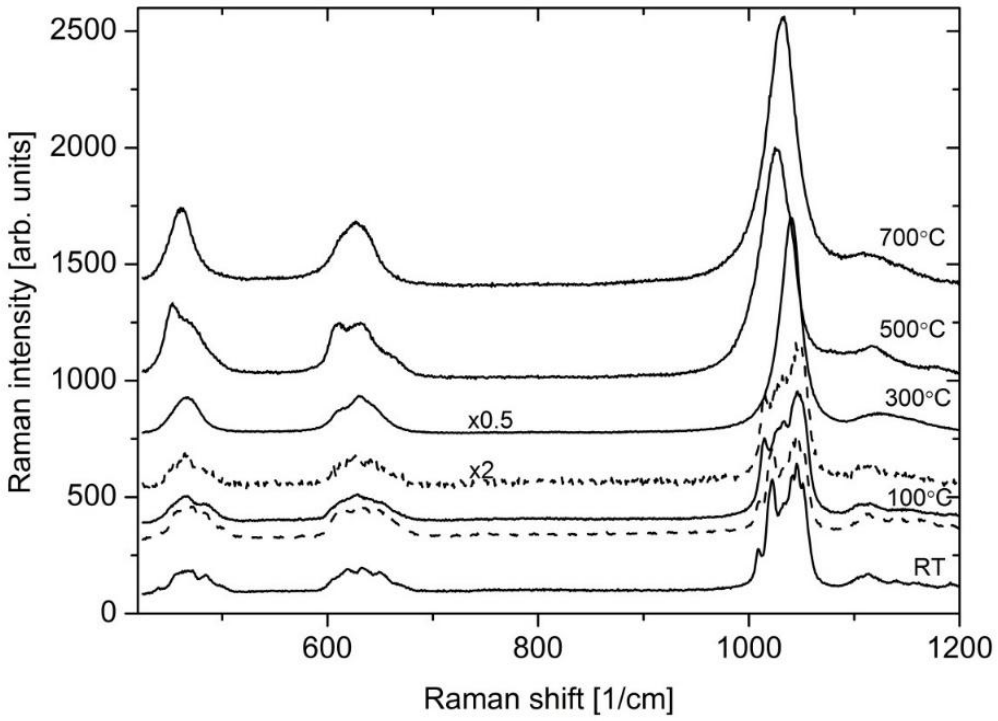

Figure 13. Thermal evolution of the Raman spectra of $Na_2Mg_2(SO_4)_3$. Dotted line, spectra at 100 ˚C and room temperature during the cooling step.

sulphate groups respectively [29]. The nature of these bands is affected by splitting or multiplication effects arising from the local symmetry of S atoms, the number of non-equivalent S sites and correlation effects. The latter are neglected because SO_4 tetrahedra are quite far away from each other and so such correlation effects, if present, are expected to be small. Local S symmetry may also break the degeneracy of ν_2, ν_3 and ν_4 bands. However, this effect is absent for the already non-degenerate A_1 bands appearing around 1040 cm^{-1}, which are attributed to the SO_4 breathing modes. Therefore, at least for these modes, the split-like aspect in the monoclinic phase comes from the occurrence of 18 different crystallographic S sites. Much simpler is the spectrum in the cubic langbeinite phase, where there is a single S site. In accordance to this, a single A_1 band is found at high temperature whereas the other bands may be split because of the local S symmetry.

Particularly interesting is the evolution of the Raman spectrum with increasing temperature (Figure 13). From this evolution, a first phase transition seems to occur at 100°C, as suggested by the disappearance or coalescence of some bands in all groups of internal modes. This spectrum at 100°C is remarkably similar to that of lightly (5%) K doped $Na_2Mg_2(SO_4)_3$, which we have shown to adopt an orthorhombic cell related to a heavily distorted langbeinite structure (to be described in a follow up paper on mixed K/Na systems [30], shown in Figure 14 for reference purposes), which leads us to propose that $Na_2Mg_2(SO_4)_3$ is transforming from monoclinic to orthorhombic symmetry.

The phase change is subtle, which may explain why the transition is not clearly observed in the variable temperature XRD study (Figure 2). At 290°C the spectrum transforms to that of the langbeinite phase, and is identical to that of the high temperature phase, allowing for thermal broadening effects. In agreement with the variable temperature XRD data, as temperature increases, the sample decomposes into

a mixture of $Na_2Mg_3(SO_4)_4$ and $Na_2Mg(SO_4)_2$ and the spectrum overlaps those of both phases. Figure 14 also includes the room temperature and 500°C spectra of both phases for reference purposes. It is interesting that the decomposition temperature (480°C) of $Na_2Mg_2(SO_4)_3$ to give $Na_2Mg_3(SO_4)_4$ and $Na_2Mg(SO_4)_2$ is significantly higher in the Raman measurements than in VTXRD (350°C). The difference is ascribed to the higher heating rates used in the Raman experiments, which help to retain the langbeinite phase to higher temperatures than in the XRD experiment. Finally, at 600°C the $Na_2Mg_3(SO_4)_4$ and $Na_2Mg(SO_4)_2$ phases recombine and the spectrum becomes that of the langbeinite $Na_2Mg_2(SO_4)_3$ phase, which is maintained on fast cooling (20°C/min) down to 250°C where it transforms to the orthorhombic phase, recovering the original monoclinic spectrum at room temperature. Once again, the relatively high cooling rates used in the Raman stage help to maintain the langbeinite phase, in this case completely avoiding the decomposition observed on cooling in the variable temperature XRD studies.

4. Conclusions

This detailed X-ray diffraction and Raman spectroscopy study of the $Na_2Mg_2(SO_4)_3$ system highlights enormous complexities within this system. We show that single phase $Na_2Mg_2(SO_4)_3$ can only be prepared by quenching/rapid cooling from high temperature, as otherwise phase decomposition to give $Na_2Mg(SO_4)_2$ and $Na_2Mg_3(SO_4)_4$ results. These complexities are highlighted by the changes observed on heating quenched $Na_2Mg_2(SO_4)_3$ to elevated temperatures, with the XRD data showing the following phase transformations:

Monoclinic $P2_1$, $Na_2Mg_2(SO_4)_3 \xrightarrow{250°C}$ Langbeinite $P2_13$, $Na_2Mg_2(SO_4)_3 \xrightarrow{350°C}$ Mixture $Na_2Mg(SO_4)_2$ and $Na_2Mg_3(SO_4)_4 \xrightarrow{575°C}$ Langbeinite $P2_13$, $Na_2Mg_2(SO_4)_3$

Moreover, Raman data suggest an additional transformation at ≈100°C to a distorted langbeinite-type phase. Overall the work highlights the interesting observation of the langbeinite structure for $Na_2Mg_2(SO_4)_3$ at elevated temperature, which is unusual given that this structure is only usually formed when larger alkali metal ions are present, and it is likely that the local strain due to the smaller Na in the langbeinite framework is responsible for the complex changes in structure/composition that are observed on heating/cooling. Overall the interesting and complex structural features for these sodium magnesium sulphate systems highlight the need for detailed structural study of other Na mixed metal sulphate systems.

Acknowledgements

We would like to thank the Bolashak International Scholarship fund (PhD scholarship for Ivan Trussov) for funding. The work has been supported by the Spanish Ministerio Economía y Competitividad and Feder funds through grant MAT2016-77769R as well. We would also like to thank the EPSRC UK National Crystallography Service at the University of Southampton for the collection of the crystallographic data on the $Na_2Mg(SO_4)_2$ system.

References

[1] J.B. Goodenough, Y. Kim, Challenges for rechargeable Li batteries, Chem. Mater. 22 (2010) 587–603. doi:10.1021/cm901452z.

[2] P. Barpanda, G. Oyama, S. Nishimura, S.-C. Chung, A. Yamada, A 3.8-V earth-abundant sodium battery electrode, Nat. Commun. 5 (2014) 1–8. doi:10.1038/ncomms5358.
[3] M. Sun, G. Rousse, M. Saubanère, M.L. Doublet, D. Dalla Corte, J.M. Tarascon, A2VO(SO4)2 (A = Li, Na) as electrodes for Li-Ion and Na-ion batteries, Chem. Mater. 28 (2016) 6637–6643. doi:10.1021/acs.chemmater.6b02759.
[4] M. Reynaud, G. Rousse, A.M. Abakumov, M.T. Sougrati, G. Van Tendeloo, J.-N. Chotard, J.-M. Tarascon, Design of new electrode materials for Li-ion and Na-ion batteries from the bloedite mineral Na 2 Mg(SO 4) 2 ·4H 2 O, J. Mater. Chem. A. 2 (2014) 2671–2680. doi:10.1039/C3TA13648E.
[5] L.L. Driscoll, E. Kendrick, A.J. Wright, P.R. Slater, Investigation into the effect on structure of oxoanion doping in Na2M(SO4)2·2H2O, J. Solid State Chem. 242 (2016) 103–111. doi:10.1016/j.jssc.2016.07.004.
[6] D. Dwibedi, R. Gond, A. Dayamani, R.B. Araujo, S. Chakraborty, R. Ahuja, P. Barpanda, Na2.32Co1.84(SO4)3as a new member of the alluaudite family of high-voltage sodium battery cathodes, Dalt. Trans. 46 (2017) 55–63. doi:10.1039/c6dt03767d.
[7] G. Oyama, S. Nishimura, Y. Suzuki, M. Okubo, A. Yamada, Off-Stoichiometry in Alluaudite-Type Sodium Iron Sulfate Na2+2xFe2−x(SO4)3 as an Advanced Sodium Battery Cathode Material, ChemElectroChem. 2 (2015) 1019–1023. doi:10.1002/celc.201500036.
[8] P. Singh, K. Shiva, H. Celio, J.B. Goodenough, Eldfellite, NaFe(SO4)2: an intercalation cathode host for low-cost Na-ion batteries, Energy Environ. Sci. 8 (2015) 3000–3005. doi:10.1039/C5EE02274F.
[9] L.L. Driscoll, A.J. Wright, P.R. Slater, Designing a facile low cost synthesis strategy for the Na–V–S–O systems, NaV(SO4)2, Na3V(SO4)3 and Na2VO(SO4)2, Dalt. Trans. 47 (2018) 13535–13542. doi:10.1039/C8DT02308E.
[10] J.B. Goodenough, H..-P. Hong, J.A. Kafalas, Fast Na+-ion transport in skeleton structures, Mater. Res. Bull. 11 (1976) 203–220. doi:10.1016/0025-5408(76)90077-5.
[11] P. Porkodi, V. Yegnaraman, P. Kamaraj, V. Kalyanavalli, D. Jeyakumar, Synthesis of NASICON · A Molecular Precursor-Based Approach, Chem. Mater. 20 (2008) 6410–6419. doi:10.1021/cm800208k.
[12] R. Perret, A. Thierrsorel, J.P. Peter, R. Masse, Triple Sulfates MIMIIMIII(SO4)3. Rhombohedral Sulfate NaMIIMII(SO4)3 (MII=Mg, Mn, Co, Ni, Zn, MIII = Al, Ga, In, Cr, Fe), Bull. La Soc. Fr. Mineral. Cristallogr. 98 (1975) 103–106.
[13] R. Perret, N. Bartil, A. Thierrsorel, Rhombohedral Sulfates AgMIICr(SO4)3, NaKMII2Cr2(SO4)6 and AgKMII2Cr2(SO4)6, MII - Mg, Mn, Co, Ni, Zn, Comptes Rendus Hebd. Des Seances L'Academie Des Sci. Ser. C. 282 (1976) 173–174.
[14] P.R. Slater, C. Greaves, Neutron diffraction structural study of the nasicon-related phases LixMIIxMIII2-x(SO4)3-y(SeO4)y (MII = Mg, Ni, Zn; MIII = Al, Cr), J. Mater. Chem. 4 (1994) 1463–1467. doi:10.1039/JM9940401463.
[15] P.R. Slater, C. Greaves, Powder neutron diffraction study of the nasicon-related phases NaxMIIxMIII2-x(SO4)3-y(SeO4)y: MII = Mg, MIII = Fe, In, J. Mater. Chem. 4 (1994) 1469–1473. doi:10.1039/JM9940401469.
[16] P.R. Slater, C. Greaves, Synthesis and Conductivities of Sulfate/Selenate Phases Related to Nasicon: NaxM′(II)xM″(III)2-x(SO4)3-y(SeO4)y, J. Solid State Chem. 107 (1993) 12–18. doi:10.1006/jssc.1993.1317.
[17] S.P. Jakobsson, E.S. Leonardsen, S.P. Jakobsson, E.S. Leonardsen, T. Balić-Žunić,

Encrustations from three recent volcanic eruptions in Iceland: the 1963–1967 Surtsey, the 1973 Eldfell and the 1991 Hekla eruptions, Fjölrit Náttúrufræðistofnunar. 52 (2008) 65.
[18] T. Balić-Žunić, R. Birkedal, A. Katerinopoulou, P. Comodi, Dehydration of blödite, Na2Mg(SO4)2(H2O)4, and leonite, K2Mg(SO4)2(H2O)4, Eur. J. Mineral. 28 (2016) 33–42. doi:10.1127/ejm/2015/0027-2487.
[19] A. Zemann, J. Zemann, Die Kristallstruktur von Langbeinit, K2Mg2(SO4)3, Acta Crystallogr. 10 (1957) 409–413. doi:10.1107/S0365110X57001346.
[20] G. Gattw, J. Zemann, Über Doppelsulfate vom Langbeinit-Typ, A2B2(SO4)3, Zeitschrift Für Anorg. Und Allg. Chemie. 293 (1958) 233–240. doi:10.1002/zaac.19582930502.
[21] I. V. Zatovsky, N.Y. Strutynska, Y.A. Hizhnyi, S.G. Nedilko, N.S. Slobodyanik, N.I. Klyui, Partial Substitution of Potassium with Sodium in the K2Ti2(PO4)3 Langbeinite-Type Framework: Synthesis and Crystalline Structure of K1.75Na0.25Ti2(PO4)3, ChemistryOpen. 7 (2018) 504–512. doi:10.1002/open.201800059.
[22] M. Hidouri, H. Jerbi, M. Ben Amara, The iron phosphate NaBaFe2(PO4)3, Acta Crystallogr. Sect. E Struct. Reports Online. 64 (2008) i51–i51. doi:10.1107/S1600536808023040.
[23] B.H. Toby, R.B. Von Dreele, GSAS-II: The genesis of a modern open-source all purpose crystallography software package, J. Appl. Crystallogr. 46 (2013) 544–549. doi:10.1107/S0021889813003531.
[24] S.J. Coles, P.A. Gale, Changing and challenging times for service crystallography, Chem. Sci. 3 (2012) 683–689. doi:10.1039/c2sc00955b.
[25] O. V. Dolomanov, L.J. Bourhis, R.J. Gildea, J.A.K. Howard, H. Puschmann, OLEX2 : a complete structure solution, refinement and analysis program, J. Appl. Crystallogr. 42 (2009) 339–341. doi:10.1107/S0021889808042726.
[26] G.M. Sheldrick, SHELXT – Integrated space-group and crystal-structure determination, Acta Crystallogr. Sect. A Found. Adv. 71 (2015) 3–8. doi:10.1107/S2053273314026370.
[27] G.M. Sheldrick, Crystal structure refinement with SHELXL, Acta Crystallogr. Sect. C Struct. Chem. 71 (2015) 3–8. doi:10.1107/S2053229614024218.
[28] F. Hatert, Na4Fe2+Fe3+(PO4)3 , a new synthetic NASICON-type phosphate, Acta Crystallogr. Sect. E Struct. Reports Online. 65 (2009) i30–i30. doi:10.1107/S1600536809009210.
[29] A. Hamilton, R.I. Menzies, Raman spectra of mirabilite, Na2SO4·10H2O and the rediscovered metastable heptahydrate, Na2SO4·7H2O, J. Raman Spectrosc. 41 (2010) 1014–1020. doi:10.1002/jrs.2547.
[30] I.A. Trussov, L.L. Driscoll, M.L. Sanjuan, L. Male, A. Orera, P.R. Slater, Synthesis and structures of sodium doped K2Mg2(SO4)3 langbeinite phases. Manuscript in preparation, n.d.